Magnetostatic Surface-Wave Transducers

JAMES C. SETHARES, MEMBER, IEEE

Abstract—**Magnetostatic surface-wave (MSSW) transducer theory is extended and generalized. A Fourier transform relation is established between MSSW field amplitudes and transducer spatial current distribution. Expressions are developed for the radiation resistance of periodic meander and grating transducers, spatial harmonic amplitudes, and radiation resistance for uniform and nonuniform current distribution models. An expression is given for the radiation resistance of apodized transducers. The results enable one to predict transducer frequency response for a specified weighting of transducer element width, length, and spacing.**

I. Introduction

PREVIOUS investigations [1]–[7] related to magnetostatic surface-wave (MSSW) technology have suggested the possibility of practical sophisticated passive microwave devices for direct signal processing at microwave frequencies. Such a technology would extend processing capabilities now performed by SAW devices at UHF frequencies into the microwave region, and would constitute a significant advance in signal-processing capabilities. A review of such magnetostatic-wave devices is provided by Collins *et al.* [7] (1977) in which the relative merits of CCD, SAW, and MSSW technologies are compared as to their time-frequency characteristics. However, very little general design theory has been available for periodic MSSW transducers. Toward this end, MSSW transducer theory is extended and generalized. Some recent work along these lines has also been done by Emtage [8] and Wu [5] *et al.* Emtage used a normal-mode approach to characterize a multielement transducer, and Wu used superposition of independent conducting strip elements. The present work provides a quantitative relation between the normal-mode approach and superposition. In addition, Emtage analyzed the interaction of a current strip with a magnetic system in terms of surface permeabilities. He defined a useful coupling constant and obtained expressions for the power carried by a running wave in a multilayer magnetic system, both in terms of surface permeabilities. The surface permeability approach is useful for analyzing multilayer magnetic systems. Wu presented expressions for the insertion loss of multielement transducer pairs, along with experimental verification of their low-loss microstrip transducer model. Here, a Fourier transform relation is established between MSSW field amplitudes and transducer spatial current distribution. Design equations are presented, including radiation resistance for periodic and nonperiodic meander and grating transducers, spatial harmonic amplitudes and radiation resistance for uniform and nonuniform current-distribution models, and radiation resistance for apodized transducers. In addition, the transducer model presented here differs from others in that the present one does not contain microstrip parameters in the expression for radiation resistance. A connection between the various models is presented.

Manuscript received May 23, 1978; revised September 13, 1978.

The author is with the Electromagnetic Sciences Division, Deputy for Electronic Technology, Rome Air Development Center, Hanscom AFB, Bedford, MA 01731.

II. Basic Theory

A. Assumptions

The system analyzed in this report is shown in Fig. 1. A transducer in the form of a meander or a grating line is excited with an RF current. Transducer connections to the ground plane structure and to input/output lines are shown in Fig. 2. Currents produce RF magnetic fields which generate a variety of propagating modes within the structure. One particular mode having potential for signal processing directly at microwave frequencies is the MSSW. This is the mode of interest here. It is nonreciprocal, propagates perpendicular to the magnetic biasing field, guided by two parallel surfaces (though they need not be precisely parallel), and its energy is concentrated near one surface. It propagates with a velocity between that of acoustic and light waves (velocity is magnetically tunable), it handles milliwatts of power, and, in practical situations, its frequency range is between 2 and 15 GHz. The mode is a coupled electromagnetic–ferromagnetic TE mode for which Maxwell's equations, the linearized gyromagnetic equation, and EM boundary conditions are simultaneously satisfied.

All important restrictions and assumptions made in the analysis are listed below.

1) End effects caused by arrays of finite extent are neglected.

2) MSSW power is calculated in the far-field region where the transducer has negligible effect on propagation modes.

3) The magnetostatic approximation $\nabla \times \vec{H} \approx 0$ is employed.

4) Nonlinear effects are neglected.

5) A two-dimensional problem with uniformity along the length of conduction strips is considered.

6) Good conductors are assumed and the thickness of conducting strips approaches zero.[1]

[1]A consequence of the small thickness t and high conductivity σ conducting strip approximation is that when $\sigma \to \infty$ skin depth $\delta \to 0$, and then two limiting cases must be considered. When $\delta \ll t$, thickness t must be assumed finite in the analyses. When $\delta \gg t$, conduction strip thickness can be neglected as is done here. As a practical matter, for aluminum at 3 GHz, $\delta \approx 1.5$ μm. In this case the present theory would be rigorous only for strip thickness much less than 1.5 μm.

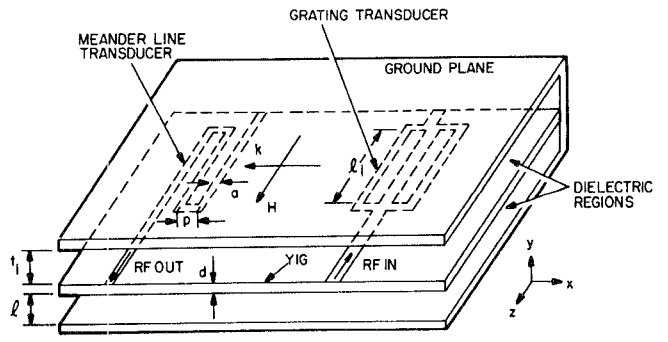

Fig. 1. MSSW delay line configuration with meander and grating line transducers on YIG and double ground planes.

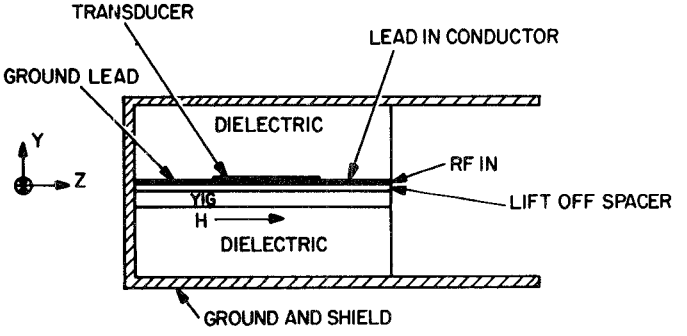

Fig. 2. Transducer connections to ground plane structure. Liftoff spacer thickness is assumed zero in this report.

7) The magnetic layer is assumed homogeneous and isotropic.

B. Form of the Electromagnetic Fields

With reference to the geometry in Fig. 3, $E_x = E_y = 0$, and $\partial/\partial z \to 0$ for all fields, and all field-component amplitudes have the form $f_k(y)\exp(i(\omega t - kx))$. The biasing field is z directed, the magnetostatic approximation $\nabla \times H \approx 0$ applies, and the nonzero RF field components H_x, H_y, B_x, B_y, and E_z satisfy the following reduced equations:

$$\frac{\partial H_y}{\partial x} - \frac{\partial H_x}{\partial y} \approx 0$$

$$\frac{\partial E_z}{\partial y} = -i\omega B_x$$

$$\frac{\partial E_z}{\partial x} = i\omega B_y$$

$$\frac{\partial B_x}{\partial x} + \frac{\partial B_y}{\partial y} = 0 \tag{1}$$

with

$$\begin{bmatrix} B_x \\ B_y \end{bmatrix} = \mu_0 \begin{bmatrix} \mu_{11} & i\mu_{12} \\ -i\mu_{12} & \mu_{22} \end{bmatrix} \begin{bmatrix} H_x \\ H_y \end{bmatrix}. \tag{2}$$

Following the analysis of Ganguly and Webb [3], GW, we construct solutions for B_y and H_x in each of the three regions and apply boundary conditions to evaluate field amplitudes. The remaining nonzero fields E_z, B_x, and H_y are known in terms of B_y and H_x through (1) and (2). We differ from GW by allowing arbitrary spatial current distributions, employ the magnetostatic approximation at the outset, and introduce a second ground plane. Part of the analysis was previously done without using the MSSW approximation, see [9].

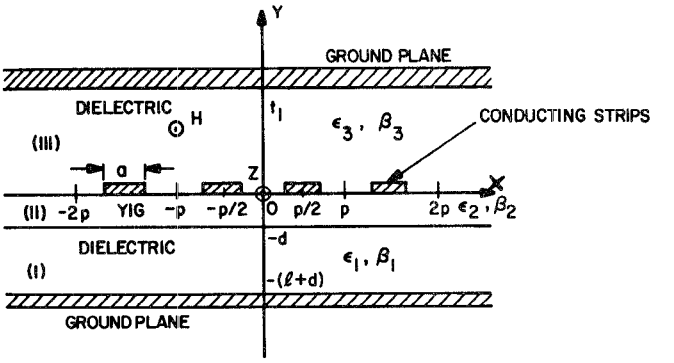

Fig. 3. Geometry of the system composed of YIG film, conducting strips, double ground plane, and dielectric regions.

The fields B_y and H_x in region q have the form [3]:

$$B_{yq} = \mu_0 \int_{-\infty}^{\infty} [\alpha_{1q} A_q \exp(\beta_q |k| y) - \alpha_{2q} B_q \exp(-\beta_q |k| y)] \exp(-ikx)\, dk$$

$$H_{xq} = -i \int_{-\infty}^{\infty} s[A_q \exp(\beta_q |k| y) + B_q \exp(-\beta_q |k| y)] \exp(-ikx)\, dk \tag{3}$$

where in the magnetostatic approximation

$$\beta_1 = \beta_3 = 1 \qquad \beta_2 = \sqrt{\mu_{22}/\mu_{11}} \equiv \beta$$

$$\alpha_{11} = \alpha_{21} = 1 \qquad \alpha_{13} = \alpha_{23} = 1$$

$$s = k/|k|, \text{ the sign of } k$$

$$\alpha_{12} \equiv \alpha_1 = \mu_{11}\beta - \mu_{12} s$$

$$\alpha_{22} \equiv \alpha_2 = \mu_{11}\beta + \mu_{12} s. \tag{4}$$

The electric field E_z in each of the three regions is obtained by multiplying the integrand of B_y by $(-\omega/k)$. H_y and B_x are obtained from B_y and H_x using the permeability matrix (2).

C. Boundary Conditions and Dispersion Relation

Application of boundary conditions determine all A_q and B_q in terms of an arbitrary surface current distribution $J(x)$. The normal component of $\vec{B}$ $(= B_y)$ vanishes at the ground planes and it is continuous at the two YIG–dielectric interfaces. Tangential component of $\vec{H}$ $(= H_x)$ is continuous along the unelectroded YIG–dielectric interface and is discontinuous by the surface current along the electroded portions of the surface. With reference to Fig. 3 and with superscripts denoting regions

$$B_y = 0, \quad \text{at } y = t_1 \quad \text{and} \quad y = -(d+l)$$

$$B_y^{\mathrm{I}} = B_y^{\mathrm{II}}, \quad \text{at } y = -d$$

$$B_y^{\mathrm{II}} = B_y^{\mathrm{III}}, \quad \text{at } y = 0$$

$$H_x^{\mathrm{I}} = H_x^{\mathrm{II}}, \quad \text{at } y = -d. \tag{5}$$

The boundary condition due to current in the periodic structure is

$$H_x^{III} - H_x^{II} = J(x), \qquad \text{at } y = 0 \tag{6}$$

where $J(x)$ is a *surface* current in the infinitely thin layer. Application of boundary conditions (5) to B_y and H_x yield the following equations relating all coefficients to B_2. Then B_2 is determined from boundary condition (6).

$$A_1 = \frac{(T+1)\exp[(\beta+1)|k|d]}{(1+\exp[-2|k|l])} B_2$$

$$B_1 = \frac{(T+1)\exp[(\beta-1)|k|d]}{\exp(2|k|l)+1} B_2$$

$$A_2 = T[\exp(2\beta|k|d)] B_2$$

$$A_3 = \frac{(\alpha_1 T\exp(2\beta|k|d) - \alpha_2)}{(1-\exp[2|k|t_1])} B_2$$

$$B_3 = \frac{(\alpha_1 T\exp[2\beta|k|d] - \alpha_2)}{\exp[-2|k|t_1]-1} B_2 \tag{7}$$

where

$$T = \frac{\alpha_2 + \tanh(|k|l)}{\alpha_1 - \tanh(|k|l)}. \tag{8}$$

Upon substitution of field expressions into (6) we obtain

$$-i\int_{-\infty}^{\infty} s[(A_3+B_3)-(A_2+B_2)]\exp(-ikx)\,dk = J(x) \tag{9}$$

and multiplying through by $e^{ik'x}$, integrating with respect to x from $-\infty$ to $+\infty$, and substituting (7) into (9), we find

$$B_2 = is\tilde{J}(k)/[2\pi F(k,\omega)] \tag{10}$$

where

$$F(k,\omega) = (\alpha_2 - \alpha_1 T\exp(2\beta|k|d))\coth(|k|t_1) - (1 + T\exp(2\beta|k|d)) \tag{11}$$

and

$$\tilde{J}(k) = \int_{-\infty}^{\infty} J(x)\exp(ikx)\,dx. \tag{12}$$

The six wave-amplitude coefficients A_1, A_2, A_3, B_1, B_2, and B_3 have now been expressed in terms of the current distribution $J(x)$ and the geometry via $F(k,\omega)$. It now remains to solve for the dispersion relation that gives k as a function of ω. In Appendix I we evaluate the integrals in (3) to obtain the fields in all regions. In carrying out the solution for the fields, we find the dispersion relation (see Appendix I, (A9))

$$e^{-2\beta|k|d} = \frac{[\alpha_2+\tanh(|k|l)][\alpha_1\coth(|k|t_1)+1]}{[\alpha_1-\tanh(|k|l)][\alpha_2\coth(|k|t_1)-1]}. \tag{13}$$

For a given frequency ω, the wavenumber k is found from (13) which is the characteristic relationship between frequency and wavenumber for the unelectroded structure consisting of YIG slab and two ground planes separated by dielectrics.

Equation (13) is generally solved numerically. When ground planes are removed, however, (t_1 and $l \to \infty$) (13) can be solved for k exactly, for a given frequency and propagation direction $s = \pm 1$. The computed k and corresponding ω values are used to calculate all field components given by (A5)–(A7) of Appendix I. We note also that all field components are proportional to G where, from (A8)

$$G = \tilde{J}(k)\exp(-\beta|k|d)/F_{TM}^{(1)}(k,\omega) \tag{14}$$

with $F_{TM}^{(1)}$ defined by (A4). The factor $\tilde{J}(k)$ is a Fourier transform (12) of an arbitrary impressed current distribution $J(x)$. This observation provides a general procedure for transducer analysis. For example, nonperiodic (or periodic) conducting strips may be driven with arbitrary current sources; then, an integration (i.e., Fourier transform) over the source distribution will yield transducer characteristics such as those given here in subsequent sections, including radiation resistance and normal-mode amplitudes.

III. Power Carried By a MSSW

With reference to Fig. 1 we calculate the far-field total power carried by a MSSW propagation in the x direction away from a transducer. The wave is bounded by the two ground planes which are located at distances t_1 and l from the YIG surfaces, and the wave is generated by an arbitrary transducer current distribution $\vec{J}(x) = \hat{z}J(x)$ A/cm.

From the $\nabla X\vec{E} = -\vec{B}$ equation

$$E_z^{(s)} = -(\omega/|k|)B_y^{(s)} \tag{15}$$

and from the permeability matrix (2)

$$H_y^{(s)} = (B_y^{(s)}/\mu_0 + i\mu_{12}H_x^{(s)})/\mu_{22}. \tag{16}$$

Power density carried by a MSSW in the x direction is equal to the real part of $p^{(s)}$, where

$$p^{(s)} = (1/2)E_z^{(s)}H_y^{(s)*} \tag{17}$$

while total power for transducer aperture width l_1 is

$$P^{(s)} = (l_1/2)\int_{-(l+d)}^{t_1} E_z^{(s)}H_y^{(s)*}\,dy. \tag{18}$$

Substitution of field expressions, from Appendix I, for $E_z^{(s)}$ and $H_y^{(s)}$ into (18) yields an expression for $P^{(s)}$, thus (see Appendix II, also)

$$P^{(s)} = \frac{\omega\mu_0 l_1}{2k_s^2}|G(k,\omega)|^2|A(k_s)| \tag{19}$$

where

$$A(k_s) = (T_M+1)^2\left[\frac{\sinh(2k_s l)/4 - k_s l/2}{\cosh^2(k_s l)}\right] + (\alpha_1 T_M e^{\beta k_s d} - \alpha_2 e^{-\beta k_s d})^2\left[\frac{\sinh(2k_s t_1)/4 - k_s t_1/2}{\sinh^2(k_s t_1)}\right] + (\alpha_1 T_M^2/2)(e^{2\beta k_s d}-1) - (\alpha_2/2)(e^{-2\beta k_s d}-1) - 2k_s d T_M \mu_{11}. \tag{20}$$

In evaluating (19), $k_s = |k|$ satisfying (13) and

$$G(k,\omega) = \tilde{J}(sk_s)e^{-\beta k_s d}/F_{TM}^{(1)}(k_s,\omega). \tag{21}$$

In order to identify a radiation resistance we write (19) as

$$P^{(s)}=(l_1/2)R_1^{(s)}\left|\tilde{J}(k)\right|^2 \tag{22}$$

where

$$R_1^{(s)}=\frac{\omega\mu_0 e^{-2\beta k_s d}}{k_s^2\left|F_{TM}^{(1)}(k_s,\omega)\right|^2}|A(k_s)|. \tag{23}$$

The function $R_1^{(s)}$ is a function of YIG parameters and ground-plane spacing t_1 and l, and it is independent of transducer parameters, while $\tilde{J}(k)$ is a spatial transform of the transducer current distribution defined by (12).

IV. Radiation Resistance for Noninteracting Electrodes and Uniform Current Model

With spatially uniform current I_0 flowing in each of N equally spaced transducer conducting strips, $\tilde{J}(k)$ can be evaluated in closed form. Consider a transducer made up of N conducting strips each of width a carrying current I_0. Define $\eta=\pm 1$. When $\eta=+1$ all conductors are connected in parallel to form a grating, and when $\eta=-1$ they are connected in series to form a meander line. The Fourier transform $\tilde{J}(k)$ of this current distribution is

$$\tilde{J}(k)=\int_{-\infty}^{\infty}J(x)e^{ikx}dx=\int_{-a/2}^{(N-1)p+a/2}J(x)e^{ikx}dx \tag{24}$$

$$\tilde{J}(k)=(I_0/a)\sum_{n=1}^{N}(\eta)^{n+1}\int_{(n-1)p-a/2}^{(n-1)p+a/2}e^{ikx}dx. \tag{25}$$

Here, the origin $x=0$ has been shifted to the center of the "first" strip. It can be shown that (25) will reduce to the following expression.

$$\tilde{J}(k)=I_0\left[\frac{\sin(ka/2)}{(ak/2)}\right]\left\{\frac{1-\eta^N e^{ikpN}}{1-\eta e^{ikp}}\right\}. \tag{26}$$

The term in braces is an array factor and the term in brackets is an element factor. For a given k number the element factor depends on stripwidth and the array factor depends on strip placement. For $N=1$ the single strip result is obtained. Substitution of (26) into (22) yields the radiation resistance, defined by

$$R_m^{(s)}\equiv 2P^{(s)}/|I_T|^2 \tag{27}$$

where

$$I_T=[(1-\eta)+(1+\eta)N]I_0/2 \tag{28}$$

is the total current into the transducer, and

$$R_m^{(s)}=\left\{\frac{2R_1^{(s)}l_1}{(1-\eta)+(1+\eta)N^2}\right\}\cdot\left[\frac{\sin(ak_s/2)}{(ak_s/2)}\right]^2\left|\frac{1-\eta^N e^{ik_s pN}}{1-\eta e^{ik_s p}}\right|^2 \tag{29}$$

where $R_1^{(s)}$ is independent of transducer parameters. The array factor in (29) will reduce when $\eta=1$ for the grating to that given by Wu *et al.* [5]. Also, when ground planes are removed, t_1 and $l\to\infty$, Wu's $Z_0\to 0$ and $\sec^2\beta l\to 1$; the two models are then identical. This provides a connection between the two models. The two models agree with experiment reasonably well and differ only in second-order effects. Moreover, when we remove a ground plane by letting l or t_1 go to infinity, and let $N=1$, we retrieve GW's radiation resistance for the single strip.

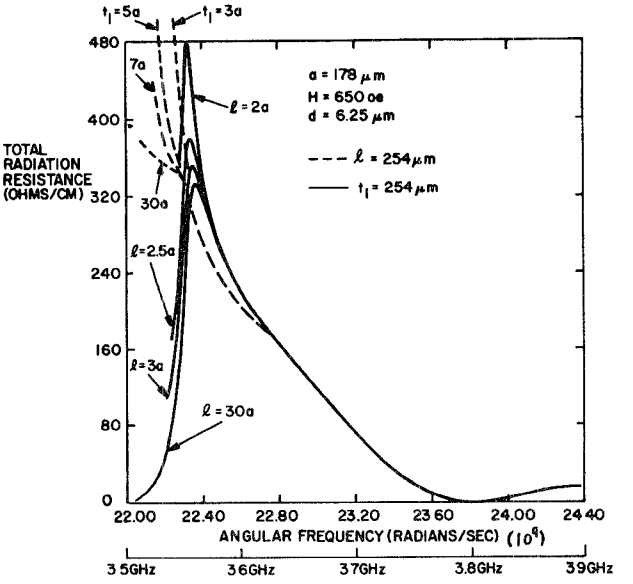

Fig. 4. Total radiation resistance per unit width as a function of frequency for a single strip and for various ground plane spacings.

For a grating, $\eta=+1$, $I_T=NI_0$, and

$$R_m^{(s)}=\frac{l_1R_1^{(s)}}{N^2}\left[\frac{\sin(ak_s/2)}{(ak_s/2)}\right]^2\left[\frac{\sin(k_spN/2)}{\sin(k_sp/2)}\right]^2. \tag{30}$$

For a meander line, $\eta=-1$, $I_T=I_0$, and with N even

$$R_m^{(s)}=l_1R_1^{(s)}\left[\frac{\sin(ak_s/2)}{(ak_s/2)}\right]^2\left[\frac{\sin(k_spN/2)}{\cos(k_sp/2)}\right]^2. \tag{31}$$

The total radiation resistance is important for matching into the transducers. Fig. 4 gives curves of total radiation resistance per unit width, $(R_m^{(+)}+R_m^{(-)})/l_1$, for the single-strip case $N=1$. $R_m^{(+)}$ and $R_m^{(-)}$ are obtained using (23) and (29). For all curves, $a=178$ μm, $H=650$ Oe, and $d=6.25$ μm. For the dashed curves $l=254$ μm and t_1 is a parameter, while for the solid curves $t_1=254$ μm and l is the parameter. The figure can be compared directly with Fig. 3 of GW. In particular, our $l=(30\ a)$ and $t_1=(30\ a)$ curves correspond to GW cases (a) and (b), respectively. They correspond exactly when $l\to\infty$ and $t_1\to\infty$.

V. Normal Modes

By expressing the current distribution in terms of space harmonics which match transducer periodicity, space-harmonic operation of MSSW transducers may be analyzed. Toward this end $J(x)$ is expressed in the uniform current model, as follows:

$$J(x)=(2I_0/p)\sum_{l'=1}^{\infty}\operatorname{sinc}(l'a/2p)\cdot[(1+\eta\cos(l'\pi))/2]\cos(l'\pi x/p) \tag{32}$$

where

$$\operatorname{sinc}(x)=[\sin(\pi x)]/(\pi x).$$

This is a rectangular function equal to I_0 and ηI_0 on alternate conducting strips, respectively, and extends from $-\infty<x<\infty$. Its fundamental period is p for a grating and $2p$ for a meander. For a transducer made up of N conducting strips over a length W in the x direction, we have from (12) and (32):

$$\tilde{J}(k)=(2I_0/p)\sum_{l'=1}^{\infty}\operatorname{sinc}(l'a/2p)[(1+\eta\cos(l'\pi))/2]\cdot\int_{-W/2}^{W/2}e^{kkx}\cos(l'\pi x/p)\,dx. \quad (33)$$

After integration we have

$$\tilde{J}(k)=i(I_0W/p)\sum_{l'=1}^{\infty}[(1+\eta\cos(l'\pi))/2]\operatorname{sinc}(l'a/2p)\cdot\left\{\frac{\sin[(k+l'\pi/p)W/2]}{(k+l'\pi/p)W/2}+\frac{\sin[(k-l'\pi/p)W/2]}{(k-l'\pi/p)W/2}\right\}. \quad (34)$$

Now, for a sufficient number of strips, $W\approx Np$, where p is the center-to-center spacing of conducting strips. For operation near any harmonic, $k\approx l'\pi/p$, only two terms in the infinite sum contribute significantly to the total $\tilde{J}(k)$, one for each sign of s, and for a wave in either direction we find from (22), (23), (27), (28), and (34) the following radiation resistance valid near any space harmonic:

$$R_m^{(s)}=\frac{R_1^{(s)}l_1[1+\eta\cos(n\pi)]N^2}{[(1-\eta)+(1+\eta)N^2]}\operatorname{sinc}^2(na/2p)\cdot\operatorname{sinc}^2[(k-n\pi/p)pN/2\pi]. \quad (35)$$

Equation (35) gives the radiation resistance for each normal mode n. When operation is at the fundamental, (29) and (35) give identical results, thus providing a quantitative relationship between the normal-mode and superposition models. For operation away from the fundamental the two, (29) and (35), radiation resistances are different. Equation (29) is based on the superposition of field amplitudes generated by isolated, independent conducting strips. Equation (35) is based on the superposition of field amplitudes generated by identical but dependent strips of an infinite array, with end effects neglected.

Because MSSW spatial harmonics are closely spaced in frequency, typically on the order of 100-MHz separation at S band, (29) is more practical to use than (35). For operation near the fundamental, however, either (29) or (35) is adequate, but when the number of strips is large (35) is more accurate because it is based on an infinite-array approximation.

We now compare (35) with Emtage's [8] (42). Take the real part of Z_t (42) and let $k\approx k_0$, i.e., operation near synchronism. We find

$$(Z_t)_{\text{REAL}}=\left[(4Rl\,N)\frac{Z_e^2}{Z_m^2}\right]\operatorname{sinc}^2(\theta N/2\pi)$$

for Emtage's radiation resistance for an N element transducer with opposing currents in adjacent lines. Now, in (35), let $\eta=-1$, $\eta=1$, $\pi/p=k_0$, $R'=R_1^{(+)}+R_1^{(-)}$, and $l_1=l$, then

$$(R_m)_{\text{TOT}}=(R'lN^2)\operatorname{sinc}^2(\theta N/2\pi)$$

where $\theta=\pi\left(\frac{k}{k_0}-1\right)$ and l here is the length of each element. These two expressions $(Z_T)_{\text{REAL}}$ and $(R_m)_{\text{TOT}}$ for radiation resistance differ by the scaling factor R'/R,

$$\frac{R'}{R}=\frac{4}{N}\left(\frac{Z_e}{Z_m}\right)^2$$

where Z_e and Z_m are microstrip parameters.

The k dependence is the same for both models, same sinc argument, which is the motivation for indentifying Emtage's results with normal-mode theory. This, then provides a connection between the two models.

Space-harmonic amplitudes may be obtained from (34). As noted previously, all field-component amplitudes are proportional to $\tilde{J}(k)$. When $\tilde{J}(k)$ is evaluated near synchronism, $k\approx n\pi/p$, the normalized field amplitude

$$\bar{A}_n\equiv|\tilde{J}(k)/(I_0N)|$$

is

$$\bar{A}_n=[(1+\eta\cos(n\pi))/2]\operatorname{sinc}(na/2p)\cdot\operatorname{sinc}[(k-n\pi/p)Np/2\pi]. \quad (36)$$

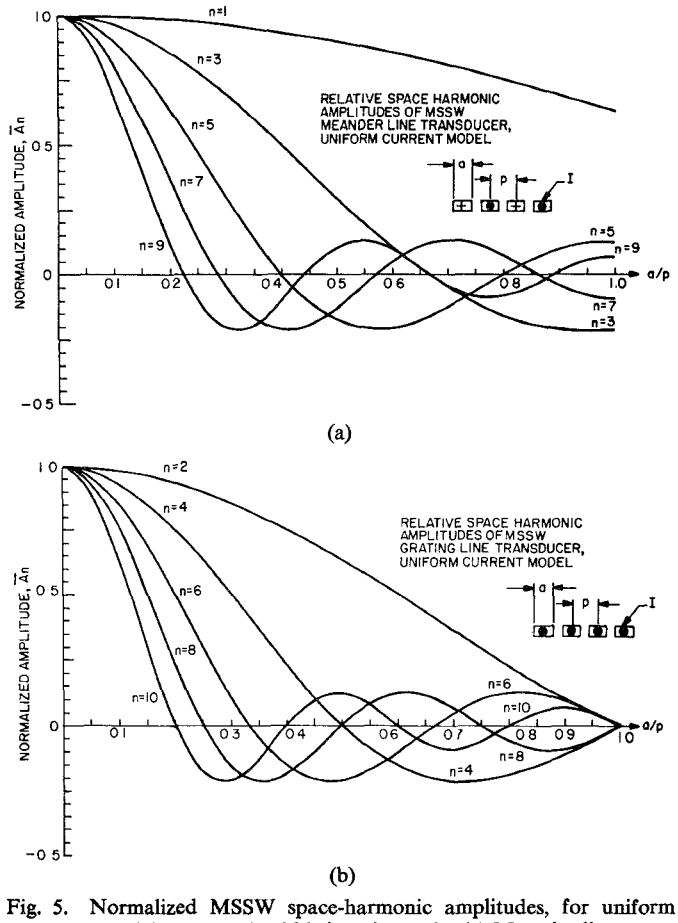

Fig. 5. Normalized MSSW space-harmonic amplitudes, for uniform current model versus stripwidth/spacing ratio. (a) Meander line transducer. (b) Grating line transducer.

Normalized amplitudes at synchronism for a meander and grating transducer are shown in Fig. 5 for the first few harmonics. It is evident that the fundamental is most efficiently generated or received with fine wire transducers, $a/p \approx 0$, at the expense of high-harmonic content. On the other hand, wide meander conducting strips $a/p \approx 1$ are less efficient MSSW generators/receivers, but the harmonic content is lower. Wide gratings, $a/p \approx 1$, are even less efficient transducers. These conclusions are based on the uniform current-distribution model. Modifications due to nonuniform current distribution are expected to be more important as operating frequency is increased. This is considered in the next section.

VI. Nonuniform Current Distribution—Meander Line

Uniform current distribution is not realistic for good conductors, and moreover, the actual distribution is affected by currents in adjacent strips. A more realistic current distribution can be obtained by applying exact boundary condition to good conductors. Such a procedure predicts current peaks at the strip edges like those indicated, for a meander line with $a/p = 1/2$, in Fig. 6. It can be shown that current distribution in a strip is governed by the following equation [10], [11]:

$$\frac{J_{LP}(x)}{J_{FF}} = \frac{\pi(a/p)}{\sqrt{2}\sqrt{\cos(2\pi x/p) - \cos(\pi a/p)}\, K[\sin(\pi a/2p)]} \tag{37}$$

where $|x| < a/2$, and harmonic amplitudes are given by

$$\bar{A}_{2n+1} = (\pi/2)\left[\frac{P_n(\cos(\pi a/p))}{K[\sin(\pi a/2p)]}\right] \cdot \operatorname{sinc}[(k-(2n+1)/p)Np/2\pi]. \tag{38}$$

These harmonic amplitudes (38) are similar to those of Engan's [12] for the interdigital transducer. In (37) subscript LP refers to Legendre Polynomial (nonuniform current-distribution model) and FF to Flat Field (uniform current-distribution model). In (38) $P_n(\cos(\pi a/p))$ are Legendre Polynomials with argument $\cos(\pi a/p)$ and $K[\sin(\pi a/2p)]$ complete elliptic integrals of the first kind with modulus $\sin(\pi a/2p)$.

Space-harmonic content is quite different for the two models, though for the fundamental the two do not differ significantly for $a/p < 1/2$. At the strip center ($x = 0$) and for $a/p = 1/2$, $J_{LP}/J_{FF} = 0.6$. This means that for $a/p < 1/2$ fundamental strengths are of the same order of magnitude for both models. Harmonic amplitudes versus a/p for the LP model are plotted in Fig. 7. For $a/p \to 1$ all curves approach zero-not shown in the figure. The models differ significantly for $a/p > 1/2$.

In Fig. 8, the first three harmonics of the LP and FF model are compared. Note that for $a/p < 1/2$ the two models are nearly equivalent for the fundamental. For $a/p \to 0$ the two models are identical. For $a/p > 1/2$ the models diverge for all harmonics. Note especially the zero

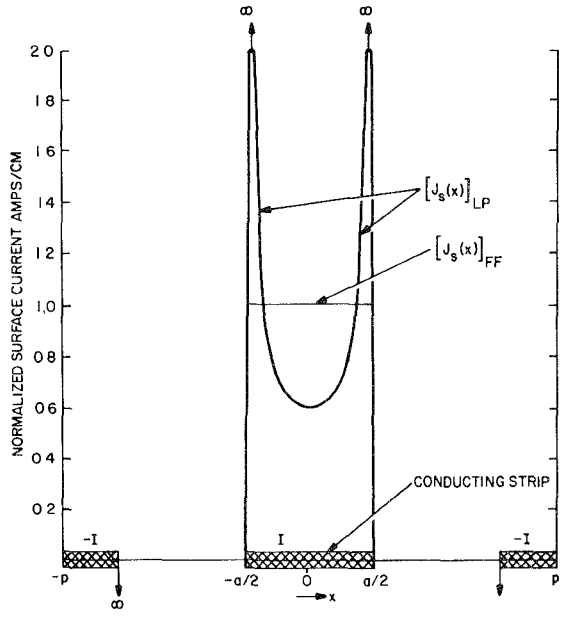

Fig. 6. Spatial current distribution in a meander line transducer conducting strip for the Flat Field (FF) model and the Legendre Polynomial (LP) model.

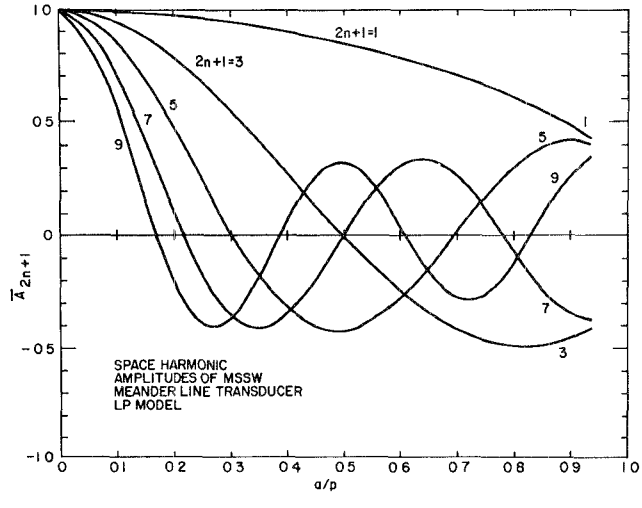

Fig. 7. Space harmonic amplitudes for MSSW meander line transducer for nonuniform current-distribution model.

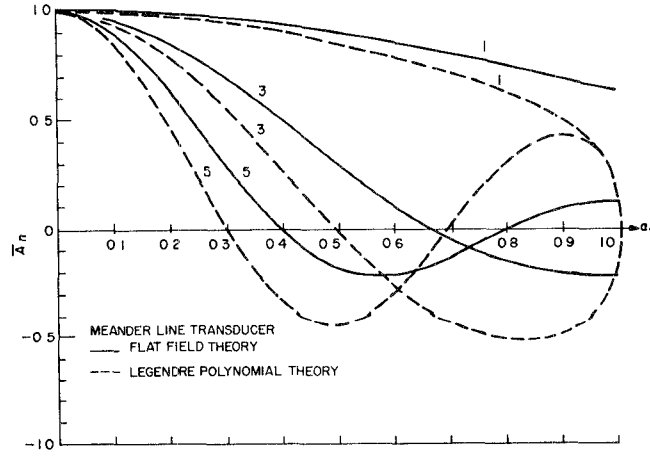

Fig. 8. Comparison of harmonic content of Flat Field and Legendre Polynomial models.

third harmonic for LP compared with about 30-percent FF third harmonic.

For interdigital and electromagnetic acoustic transducers, the LP theory is in better agreement with experiment than the FF theory [11], [13]. For fundamental frequency operation, however, the FF theory is adequate when $a/p<1/2$.

VII. Apodization of the Fundamental Normal Mode

By analogy with electromagnetic acoustic and interdigital transducer apodization theory [14], the radiation resistance for weighted, nonperiodic, and apodized MSSW transducers with varying stripwidths, separations and lengths, respectively, can be written as follows:

$$R_m^{(s)}=\frac{R_1^{(s)}}{C(\eta,N)}\left|\sum_{n=1}^{N}\operatorname{sinc}\left[2a_n/p_n(3-\eta)\right]\cdot\operatorname{sinc}\left[\frac{k_s p_n}{2\pi}-(3+\eta)/4\right]\eta^n\sqrt{l_n}\;e^{-ik_s p_n n}\right|^2 \quad (39)$$

where

$$c(\eta,N)=\left[(1-\eta)+(1+\eta)N^2\right]/2.$$

In general, there are N conducting strips, each with different width a_n, center-to-center spacing p_n and length l_n. The relation between k_s and ω, H, M, l, t_1 is given by (13), and it is independent of transducer geometry.

Equation (39) is the apodized form of (35), the normal-mode radiation resistance. The apodized form of (29), the independent conducting strip model, has been presented elsewhere [15]. Equation (39) is important for predicting bandpass filter response, with a specified weighting of transducer element length, width, and element spacing. The inverse problem of predicting transducer element weighting in order to achieve a specified filter response will require further investigation.

VIII. Conclusion

The equations presented here aid in MSSW transducer optimization. Effects of varying stripwidth, center-to-center spacing, striplength, and number of conducting strips have been determined. The apodization equation should be useful for tailoring the fundamental transducer response. A quantitative relationship between a normal mode and a superposition model has been established.

Appendix I
Evaluation of Fields

The integrals over k in (3) are performed using residue theory for which

$$\frac{\partial}{\partial k}\left[F_T(k,\omega)\right]$$

is required, where

$$F_T(k,\omega)\equiv\left[\exp(-2\beta|k|d)\right]F(k,\omega). \quad (A1)$$

Using (11) we have

$$F_T(k,\omega)=\left[\alpha_2\exp(-2\beta|k|d)-\alpha_1 T\right]\coth(|k|t_1)-\left[\exp(-2\beta|k|d)+T\right]. \quad (A2)$$

Upon differentiation of $F_T(k,\omega)$ with respect to k, and defining this derivative to be $F_{TM}^{(1)}(k,\omega)$, that is

$$F_{TM}^{(1)}(k,\omega)\equiv\frac{\partial}{\partial k}\left[F_T(k,\omega)\right] \quad (A3)$$

we find

$$F_{TM}^{(1)}=s\Bigg\{t_1(\alpha_1 T_M-\alpha_2\exp(-2\beta|k|d))\operatorname{csch}^2(|k|t_1)+2d\beta\left[1-\alpha_2\coth(|k|t_1)\right]\exp(-2\beta|k|d)-\frac{2\mu_{11}\beta l\left[\alpha_1\coth(|k|t_1)+1\right]\operatorname{sech}^2(|k|l)}{\left[\alpha_1-\tanh(|k|l)\right]^2}\Bigg\}. \quad (A4)$$

Here T_M is equal to T (8) evaluated at the magnetostatic wavenumbers obtained from $F_T(k,\omega)=0$, (A2). These wavenumber values produce poles in the integrands of (3). This can be seen from (10) wherein $B_2\to\infty$ when $F(k,\omega)\to 0$, and for finite k values $F(k,\omega)\to 0$, when $F_T(k,\omega)\to 0$ from (A1).

Evaluation of the integrals, in (3), for each of the three regions by integration along a path enclosing the upper half plane of complex k space yields the complex amplitude of MSSW's in either direction ($s=\pm 1$), as follows:

Region I

$$B_y^{(s)}=-s\mu_0 G(T_M+1)\frac{\sinh\left[|k|(y+d+l)\right]}{\cosh(|k|l)}$$

$$H_x^{(s)}=iG(T_M+1)\frac{\cosh\left[|k|(y+d+l)\right]}{\cosh(|k|l)}. \quad (A5)$$

Region II

$$B_y^{(s)}=-s\mu_0 G\left[\alpha_1 T_M\exp(\beta|k|(y+d))-\alpha_2\exp(-\beta|k|(y+d))\right]$$

$$H_x^{(s)}=iG\left[T_M\exp(\beta|k|(y+d))+\exp(-\beta|k|(y+d))\right]. \quad (A6)$$

Region III

$$B_y^{(s)}=-s\mu_0 G\left[\alpha_1 T_M\exp(\beta|k|d)-\alpha_2\exp(-\beta|k|d)\right]\frac{\sinh\left[|k|(t_1-y)\right]}{\sinh(|k|t_1)}$$

$$H_x^{(s)}=-iG\left[\alpha_1 T_M\exp(\beta|k|d)-\alpha_2\exp(-\beta|k|d)\right]\frac{\cosh\left[|k|(t_1-y)\right]}{\sinh(|k|t_1)} \quad (A7)$$

where

$$G=\left(\tilde{J}(k)\exp(-\beta|k|d)\right)/F_{TM}^{(1)}(k,\omega) \tag{A8}$$

with the constraint $F_T(k,\omega)=0$. Setting (A1) equal to zero and using (8) yields the dispersion relation

$$e^{-2\beta|k|d}=\frac{\left[\alpha_2+\tanh(|k|l)\right]\left[\alpha_1\coth(|k|t_1)+1\right]}{\left[\alpha_1-\tanh(|k|l)\right]\left[\alpha_2\coth(|k|t_1)-1\right]}. \tag{A9}$$

A common factor $\exp[i(\omega t-kx)]$ should be included in all field components. For a given frequency ω, the wavenumber k is found from (A9), which is the characteristic relationship between frequency and wavenumber for the unelectroded structure consisting of YIG slab and two ground planes separated by dielectrics.

Appendix II
Evaluation of Total Power

From (18)

$$P^{(s)}=\left(\frac{l_1}{2}\right)\int_{-(l+d)}^{t_1}E_z^{(s)}H_y^{(s)*}\,dy \tag{B1}$$

$$P^{(s)}=\frac{l_1}{2}\left\{\int_{-(l+d)}^{-d}\left[E_z^{(s)}H_y^{(s)*}\right]_{\mathrm{I}}dy+\int_{-d}^{0}\left[E_z^{(s)}H_y^{(s)*}\right]_{\mathrm{II}}dy+\int_{0}^{t_1}\left[E_z^{(s)}H_y^{(s)*}\right]_{\mathrm{III}}dy\right\}. \tag{B2}$$

Subscripts I, II, and III indicate regions. In all three regions (15) for $E_z^{(s)}$ is used. In regions I and III $H_y^{(s)}=B_y^{(s)}/\mu_0$, and in region II $H_y^{(s)}$ is given by (16). Then

$$P^{(s)}=-\frac{\omega}{|k|}\left(\frac{l_1}{2}\right)\frac{1}{\mu_0}\left\{\int_{-(l+d)}^{-d}|B_y^{(s)}|_{\mathrm{I}}^2\,dy+\frac{1}{\mu_{22}}\int_{-d}^{0}\left[|B_y^{(s)}|^2-i\mu_{12}\mu_0B_y^{(s)}H_x^{(s)*}\right]_{\mathrm{II}}dy+\int_{0}^{t_1}|B_y^{(s)}|_{\mathrm{III}}^2\,dy\right\}. \tag{B3}$$

Substitution of (A5)–(A7) into (B3) yields the desired expression (19) for total power.

Acknowledgment

The author is indebted to T. L. Tsai, Raytheon Corporation, for his contributions to the basic theory, T. L. Szabo, RADC/EEA, for helpful discussions on apodization theory, I. Koltunov, ARCON Corporation, for skillful programming, and to the RADC Antennas and RF Components Branch, for supporting the work.

References

[1] W. L. Bongianni, "Magnetostatic propagation in a dielectric layered structure," *J. Appl. Phys.*, vol. 43, pp. 2541–2548, 1972.

[2] J. B. Merry and J. C. Sethares, "Low loss magnetostatic surface waves at frequencies up to 15 GHz," *IEEE Trans. Magn.*, vol. MAG-9, pp. 527–529, Sept. 1973.

[3] A. K. Ganguly and D. C. Webb, "Microstrip excitation of magnetostatic surface waves," *IEEE Trans. Microwave Theory Tech.*, vol. MTT-23, pp. 998–1006, Dec. 1975.

[4] H. L. Glass and M. T. Elliot, "Attainment of the intrinsic FMR linewidth in YIG films grown by LPE," *J. Cryst. Growth*, vol. **34**, pp. 285–288, 1976.

[5] H. J. Wu, C. V. Smith, J. H. Collins, and J. M. Owens, "Bandpass filtering with multibar magnetostatic-surface-wave microstrip transducers," *Electron. Lett.*, vol. 13, no. 20, vol. 29, pp. 610–611, Sept. 1977.

[6] J. D. Adam, R. W. Patterson, and T. W. O'Keefe, "Magnetostatic wave interdigital transducers," presented at 23d Annual Conf. Magnetism and Magnetic Materials, paper no. 5D-4, Minneapolis, MN, Nov. 1977.

[7] J. H. Collins, J. M. Owens, and C. V. Smith, Jr., "Magnetostatic wave signal processing," in *1977 IEEE Ultrasonics Symp. Proc.*, (IEEE Cat. 77 CH1264-1SU).

[8] P. R. Emtage, "Interaction of Magnetostatic Waves with a Current," *J. Appl. Phys.*, vol. 49, p. 4475, Aug. 1978.

[9] J. C. Sethares, T. Tsai, and I. Koltvnov, "Periodic Magnetostatic Surface Wave Transducers," RADC-TR-78-78, Apr. 1978.

[10] J. C. Sethares, H. M. Frost, and T. L. Szabo, "Fields of flat conductor electromagnetic surface acoustic wave transducers," *IEEE Trans. Sonics Ultrason.*, vol. SU-24, Mar. 1977.

[11] J. C. Sethares and T. L. Szabo, "A new model for the flat conductor electromagnetic SAW transducer," *J. Appl. Phys.*, vol. 49(3), pp. 1054–1060, Mar. 1978.

[12] H. Engan, "Excitation of elastic waves by spatial harmonics of interdigital transducers," *IEEE Trans. Electron Devices*, vol. ED-16, pp. 1014, Dec. 1969.

[13] T. L. Szabo and J. C. Sethares, "Harmonic operation of SAW electromagnetic transducers," in *1977 IEEE Ultrasonics Symp. Proc.* (IEEE Cat. 77 CH1264-1SU).

[14] T. L. Szabo, "Advanced SAW Electromagnetic transducer design," in *1976 IEEE Ultrasonics Symp. Proc.*, (IEEE Cat. 76 CH1120-5SU).

[15] J. C. Sethares and I. J. Weinberg, "Apodization of variable coupling magnetostatic surface wave transducers," *J. Appl. Phys.*, vol. 50, no. 3, p. 2458, 1979.